PHYSICAL REVIEW B VOLUME 32, NUMBER 6 15 SEPTEMBER 1985

Excitons and polaritons in InP

H. Mathieu, Y. Chen, J. Camassel, and J. Allegre
Groupe d'Etude des Semiconducteurs, Université des Sciences et Techniques du Languedoc, F-34060 Montpellier Cedex, France

D. S. Robertson
Royal Signals and Radar Establishment, Saint Andrews Road, Great Malvern, Worcestershire WR14 3PS, United Kingdom
(Received 7 November 1984)

We report an investigation of the reflectivity spectra of InP at normal incidence, at pumped-helium temperature, and under [100] uniaxial stress. Three transverse exciton frequencies associated to the $1s$ ground state and the $2s$ and $3s$ excited states have been found. We deduce an exciton binding energy $E_{ex}=5.1\pm0.1$ meV. From a detailed investigation of the $1s$ ground state in terms of the three-branch polariton dispersion curves we achieve a very satisfactory agreement between theory and experiment. Resolving the fine structure of the exciton ground state, we find (i) the exchange energy $\Delta=0.04\pm0.02$ meV and (ii) the longitudinal-transverse splitting $E_{LT}=0.17\pm0.02$ meV. The surface dead layer which corresponds with the best experimental fit is twice the exciton Bohr radius, as expected for an intrinsic surface-exciton-free layer.

I. INTRODUCTION

The fine structure of excitons in semiconductors is driven both by the Coulomb interaction and the electron-hole exchange interaction. The Coulomb interaction gives rise to a Rydberg series whose energy spacing in usual III-V compounds is of the order of a few milli-electron-volts between the fundamental and the first excited state of the complex. The exchange interaction, which depends on the overlap between the electron and the hole wave functions, is lower. It is typically of the order of a tenth of a milli-electron-volt; therefore in most cases the corresponding splitting is not found within the experimental uncertainty. This exchange interaction is well characterized only for bound-exciton complex[1] because a bound exciton is atomiclike in nature and results in very sharp absorption and luminescence lines. In this case the application of external perturbations, which cause deep changes in the level scheme and oscillator strength of the system, easily allow the determination of all parameters which fit the description of the energy spectrum of the complex. In this way magnetic field[1] and uniaxial-stress experiments[2–5] have been widely used over the last years.

Concerning now the free-exciton spectrum, the situation is more controversial. In recent measurements performed under uniaxial stress,[6] the fine structure was claimed to have been resolved by extrapolation of the splitting pattern down to zero stress. In this analysis the position of the reflectance minima was plotted as a function of external stress. However, only the longitudinal-exciton resonance frequency approximately corresponds to the reflectivity minimum, whereas the important transverse resonance frequency cannot be determined so easily. On the other hand, the energy shift of the longitudinal resonance frequency differs from the one of the transverse resonance frequency.[7,8] In this case there is a subtle problem of line shape in the reflectance spectrum, especially when several resonances exist within a small energy range and one should take the analyzed values of exchange splitting of the exciton ground state with reservation. A line-shape analysis of reflectance is often necessary in order to obtain detailed information about the internal structure of the exciton states, but in the case of III-V compounds with a fourfold-degenerate valence band a complete analysis of the data must include (i) the three-mode polariton (two-mode exciton), (ii) the k-dependent energy and oscillator strengths, (iii) the perturbation-dependent energy and oscillator strengths, (iv) an exciton-free surface layer, and (v) a finite lifetime of the excitons.

In this paper we present results obtained on InP. The outline of the paper is as follows: In Sec. II we give a theoretical calculation of the exciton and polariton dispersion curves, taking into account the fourfold degeneracy of the Γ_8 valence band, the electron-hole exchange energy, and the presence of an external stress. We calculate the corresponding reflectivity spectra, taking into account an exciton-free surface layer, additional boundary conditions, and stress dependence of both the energy levels and oscillator strengths. In Sec. III we explain our experimental conditions. In Sec. IV we present our experimental results and the numerical values of the parameters which give the best fit within the model detailed in Sec. II. We discuss these values in Sec. V and present our conclusions in Sec. VI.

II. THEORY

A. Exciton dispersion curves under uniaxial stress

1. Exciton states in the center of the Brillouin zone

Basically the free-exciton ground-state in a direct-band-gap III-V compound semiconductor is made of an electron, with spin $s=\frac{1}{2}$ associated with the Γ_6 conduction-band minimum, and a hole, with angular momentum $j=\frac{3}{2}$, associated with the Γ_8 valence-band

maximum. The exchange interaction which depends upon the electron-hole overlap splits the corresponding eightfold-degenerate state characterized by the zeroth-order wave functions $|\frac{3}{2},m_h\rangle\,|\frac{1}{2},m_e\rangle$. The short-range part of the exchange effect gives rise to the $J=1$ triplet state (dipole allowed) and the $J=2$ quintuplet state (dipole forbidden). The energy difference between these two states is the so-called exchange energy Δ. Next, the long-range part of the exchange effect leads to the longitudinal-transverse splitting of the dipole-allowed state and results in a longitudinal exciton $|1,0\rangle$ and two transverse ones $|1,\pm1\rangle$. The energy difference between these two states is the so-called longitudinal-transverse splitting $E_{\rm LT}$. The exchange interaction Hamiltonian can be written in a phenomenological way:[9]

$$H_{\rm exch}=\tfrac{1}{8}\Delta(3-4JS)+E_{\rm LT}\delta_{J,1}(\delta_{M,0}-\tfrac{1}{3})\ .$$

The resulting configuration is given in Fig. 1(a), where the experimentally attainable parameter $\delta=E(1,\pm1)-E(2,m)$ is given by $\delta=\Delta-\frac{1}{3}E_{\rm LT}$. Now, following the discussion of Bonneville and Fishman,[10] the splitting $E_{\rm LT}$ only preserves the center of gravity of the triplet state for Frenkel excitons. This is no longer true for delocalized Wannier excitons. In this case the center of gravity of the triplet state is not conserved and more likely the longitudinal-transverse splitting corresponds to a shift toward higher energy of the $|1,0\rangle$ longitudinal exciton. The resulting energy-level diagram is given in Fig. 1(b), and here $\delta=\Delta$. This is the model we use for InP.

The fivefold-degenerate $J=2$ states can, in principle, split into twofold- (Γ_3) and threefold- (Γ_4) degenerate levels, due to the cubic crystal field. This splitting, which requires higher-order spin mixing in the Bloch functions, has never been observed.

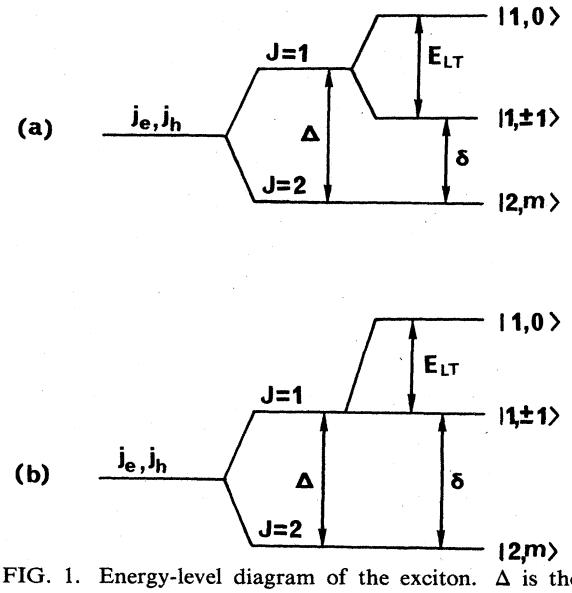

FIG. 1. Energy-level diagram of the exciton. Δ is the exchange energy, $E_{\rm LT}$ is the longitudinal-transverse splitting. (a) Frenkel excitons and (b) Wannier excitons.

2. *Exciton dispersion curves*

The problem of the exciton dispersion curves is easily solved in the case of nondegenerate bands by the well-known center-of-mass transformation. Unfortunately, in zinc-blende–type semiconductors, the valence-band maximum is fourfold degenerate at the Γ point, and the problem has no analytical solution. This has been investigated by Kane[11] for direct semiconductors and extended to indirect ones by Altarelli and Lipari.[12] Kane considers separately the low- and high-momentum limits. In the former one, which corresponds to the experimental situation in polariton experiments, he develops the exciton wave function in the eight-dimensional space of the $k=0$ exciton ground state and solves the problem using a perturbation approach. In this calculation the exchange interaction between electron and hole has not been taken into consideration. Most of Kane's results which are useful in studying the polariton dispersion curve are reviewed by Sermage and Fishman,[13] who introduced the exchange interaction. We do not repeat all the details of the calculation but only recall the resulting kinetic and exchange Hamiltonian in the base of the $|J,M_J\rangle_k$ states quantized along the wave-vector direction:

$$\begin{array}{c|ccccc}
 & |1,\pm1\rangle_k & |2,\pm1\rangle_k & |1,0\rangle_k & |2,0\rangle_k & |2,\pm2\rangle_k \\ \hline
 & \frac{1}{4}(E_l+3E_h)+\delta & \mp\frac{\sqrt{3}}{4}(E_l-E_h) & 0 & 0 & 0 \\
 & \mp\frac{\sqrt{3}}{4}(E_l-E_h) & \frac{1}{4}(3E_l+E_h) & 0 & 0 & 0 \\
 & 0 & 0 & E_l+\delta+E_{\rm LT} & 0 & 0 \\
 & 0 & 0 & 0 & E_h & 0 \\
 & 0 & 0 & 0 & 0 & E_h
\end{array} \qquad (1)$$

All the parameters have the meaning given in Ref. 13. The origin of the energies is taken on the $|2,m\rangle$ states at $k=0$. δ is the splitting $E(1,\pm1)$-$E(2,m)$ and corresponds to the exchange energy Δ as already discussed for Wannier excitons [see Fig. 1(b)]:

$$E_l=\frac{\hbar^2k^2}{2M_l},\quad E_h=\frac{\hbar^2k^2}{2M_h}\ .$$

M_l and M_h are the effective masses of light and heavy excitons, respectively, which correspond to

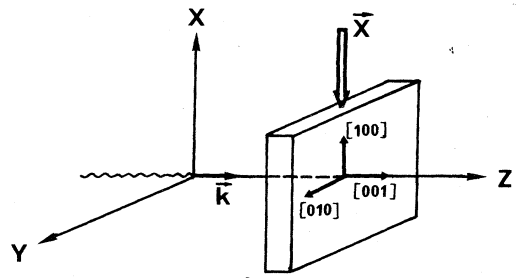

FIG. 2. Experimental configuration. **k** is the incident photon wave vector. **X** is the stress direction. Light with electric field along X (Y) axis corresponds to π (σ) polarization with respect to the stress.

$$\frac{1}{M_1}=\frac{1}{M_a}+\frac{1}{M_c},\quad \frac{1}{M_h}=\frac{1}{M_a}-\frac{1}{M_c},$$

where M_a and M_c are given as a function of electron effective mass and valence-band parameters γ_i by Eqs. (66) and (67) in Ref. 11.

The $|J,M_J\rangle$ basis states are built of linear combinations of the zeroth-order basis states $|\frac{3}{2},m_h\rangle\,|\frac{1}{2},m_e\rangle$, hereafter labeled $|m_h,m_e\rangle$. The coefficients of the different combinations are the Clebsch-Gordan coefficients. For $J=1$,

$$|1,\pm1\rangle=\mp\tfrac{1}{2}\,|\pm\tfrac{1}{2},\pm\tfrac{1}{2}\rangle\pm\frac{\sqrt{3}}{2}\,|\pm\tfrac{3}{2},\mp\tfrac{1}{2}\rangle\,, \tag{2a}$$

$$|1,0\rangle=-\frac{1}{\sqrt{2}}\,|-\tfrac{1}{2},\tfrac{1}{2}\rangle+\frac{1}{\sqrt{2}}\,|\tfrac{1}{2},-\tfrac{1}{2}\rangle\,, \tag{2b}$$

and for $J=2$,

$$|2,\pm2\rangle=|\pm\tfrac{3}{2},\pm\tfrac{1}{2}\rangle\,, \tag{2c}$$

$$|2,\pm1\rangle=\frac{\sqrt{3}}{2}\,|\pm\tfrac{1}{2},\pm\tfrac{1}{2}\rangle+\tfrac{1}{2}\,|\pm\tfrac{3}{2},\mp\tfrac{1}{2}\rangle\,, \tag{2d}$$

$$|2,0\rangle=\frac{1}{\sqrt{2}}\,|-\tfrac{1}{2},\tfrac{1}{2}\rangle+\frac{1}{\sqrt{2}}\,|\tfrac{1}{2},-\tfrac{1}{2}\rangle\,. \tag{2e}$$

3. *Stress dependence*

When a uniaxial stress is applied to the crystal, the stress dependence of all $|m_h,m_e\rangle$ zero-order states is obtained by just adding the stress dependence of the constitutive particles. For InP these stress dependences are well known,[14] but the strain-matrix Hamiltonian is diagonal only if the quantization axis of the angular momentum corresponds to the stress axis. In this case the strain-matrix Hamiltonian is written as

$$\begin{array}{cc} |\pm\frac{3}{2},m_e\rangle_x & |\pm\frac{1}{2},m_e\rangle_x \\ \begin{bmatrix} A+\epsilon & 0 \\ 0 & A-\epsilon \end{bmatrix} & \end{array}\,. \tag{3}$$

A is the hydrostatic component given by $A=a(S_{11}+2S_{12})X$, where a is the hydrostatic deformation potential of the exciton; S_{ij} are the elastic compliance constants and X is the stress magnitude taken to be negative for a compression; ϵ is the shear-strain dependence of the hole. Depending on the stress direction, the magnitude of ϵ is given by the well-known expressions

$$\epsilon_{100}=b(S_{11}-S_{12})X \quad \text{for } \mathbf{X}\|[100]\,, \tag{4a}$$

$$\epsilon_{111}=\frac{d}{2\sqrt{3}}S_{44}X \quad \text{for } \mathbf{X}\|[111]\,, \tag{4b}$$

$$\epsilon_{110}=\tfrac{1}{2}(\epsilon_{100}^2+3\epsilon_{111}^2)^{1/2} \quad \text{for } \mathbf{X}\|[110]\,. \tag{4c}$$

Now remember that the kinetic and exchange Hamiltonian given in Eq. (1) was expressed in the $|J,M_J\rangle_k$ basis taking the wave vector **k** as the quantization axis while, in Eq. (3), the quantization axis corresponds to the stress direction. Since both directions do not coincide we must rotate one Hamiltonian.

Our experimental configuration corresponds with a (001) epitaxial layers. The incident light is normal to the surface so that $\mathbf{k}\|[001]$, and the stress is applied in the plane of the sample along the [100] crystallographic direction (see Fig. 2). As a result we must calculate the [100] stress Hamiltonian in the basis of the $|m_h,m_e\rangle_{001}$ states. A straightforward calculation gives

$$\begin{array}{cc} |\pm\frac{3}{2},m_e\rangle_k & |\pm\frac{1}{2},m_e\rangle_k \\ \begin{bmatrix} A+\frac{1}{2}\epsilon & -\frac{\sqrt{3}}{2}\epsilon \\ -\frac{\sqrt{3}}{2}\epsilon & A-\frac{1}{2}\epsilon \end{bmatrix} & \end{array}\,, \tag{5}$$

where $\epsilon=\epsilon_{100}=b(S_{11}-S_{12})X$.

Now we calculate the strain Hamiltonian in the $|J,M_J\rangle_k$ basis states by using Eq. (2). Next, by summing the resulting strain matrix with the matrix equation (1), we obtain the complete matrix Hamiltonian in the $|J,M_J\rangle_k$ basis. Lastly, conserving k as the quantization axis and taking account of the cubic symmetry, we define a new set of basis states which behave as p- or d-like states.

$$|X\rangle=\frac{1}{\sqrt{2}}(|1,1\rangle-|1,-1\rangle)\,, \tag{6a}$$

$$|Y\rangle=\frac{1}{\sqrt{2}}(|1,1\rangle+|1,-1\rangle)\,, \tag{6b}$$

$$|Z\rangle=|1,0\rangle\,, \tag{6c}$$

$$|2,1^+\rangle=\frac{1}{\sqrt{2}}(|2,1\rangle+|2,-1\rangle)\,, \tag{6d}$$

$$|2,1^-\rangle=\frac{1}{\sqrt{2}}(|2,1\rangle-|2,-1\rangle)\,, \tag{6e}$$

$$|2,0\rangle=|2,0\rangle\,, \tag{6f}$$

$$|2,2^+\rangle=\frac{1}{\sqrt{2}}(|2,2\rangle+|2,-2\rangle)\,, \tag{6g}$$

$$|2,2^-\rangle=\frac{1}{\sqrt{2}}(|2,2\rangle-|2,-2\rangle)\,. \tag{6h}$$

$\lvert X\rangle$	$\lvert 2,1^+\rangle$	$\lvert Y\rangle$	$\lvert 2,1^-\rangle$	$\lvert Z\rangle$	$\lvert 2,2^-\rangle$	$\lvert 2,0\rangle$	$\lvert 2,2^+\rangle$
$\frac{E_l+3E_h}{4}+\delta+A-\epsilon$	$-\frac{\sqrt{3}}{4}(E_l-E_h)$	0	0	0	0	0	0
$-\frac{\sqrt{3}}{4}(E_l-E_h)$	$\frac{3E_l+E_h}{4}+A+\epsilon$	0	0	0	0	0	0
0	0	$\frac{E_l+3E_h}{4}+\delta+A+\frac{\epsilon}{2}$	$-\frac{\sqrt{3}}{4}(E_l-E_h)-\frac{\sqrt{3}}{2}\epsilon$	0	0	0	0
0	0	$-\frac{\sqrt{3}}{4}(E_l-E_h)-\frac{\sqrt{3}}{2}\epsilon$	$\frac{3E_l+E_h}{4}+A-\frac{\epsilon}{2}$	0	0	0	0
0	0	0	0	$E_l+\delta+E_{LT}+A+\frac{\epsilon}{2}$	$-\frac{\sqrt{3}}{2}\epsilon$	0	0
0	0	0	0	$-\frac{\sqrt{3}}{2}\epsilon$	$E_h+A-\frac{\epsilon}{2}$	0	0
0	0	0	0	0	0	$E_h+A+\frac{\epsilon}{2}$	$\frac{\sqrt{3}}{2}\epsilon$
0	0	0	0	0	0	$\frac{\sqrt{3}}{2}\epsilon$	$E_h+A-\frac{\epsilon}{2}$

(7)

In this basis the kinetic-exchange-strain Hamiltonian may be written as shown at left. We obtain four 2×2 matrices which give rise to eight exciton dispersion curves. The only ones which couple with light are those containing $|X\rangle$ or $|Y\rangle$ basis function, corresponding to the different eigenvalues of the first 2×2 matrices.

For zero stress and $\mathbf{k}=\mathbf{0}$ only the $|1,\pm1\rangle$ states would couple with light, the $|X\rangle$ excitons being allowed with light polarized parallel to the [100] crystallographic axis and the $|Y\rangle$ excitons with light polarized parallel to the [010] crystallographic axis.

For zero stress but finite $\mathbf{k}$ values, the kinetic part of the Hamiltonian mixes the d-like $|2,1^+\rangle$ and $|2,1^-\rangle$ states with the $|X\rangle$ and $|Y\rangle$ states, respectively. Four states now appear that are dipole allowed. $|Z\rangle$ denotes longitudinal excitons and remains uncoupled with light. The first two matrices being identical, the corresponding eigenvalues are twofold degenerate. This gives rise to a two-branch exciton dispersion curve coupled with light and, therefore, a three-branch polariton dispersion curve.

For finite-stress and finite-$\mathbf{k}$ values we do not find any additional coupling with the $|X\rangle$ and/or $|Y\rangle$ dipole-allowed basis states, but the first two matrices are no longer equivalent. They lead to a four-branch exciton dispersion curve (dipole allowed) and then a five-branch polariton dispersion curve. Please note that the eigenstates of the first 2×2 matrix contain $|X\rangle$-like basis states and then couple with light polarized parallel to the stress axis (π polarization). On the other hand, the eigenstates of the second 2×2 matrix contain only $|Y\rangle$-like basis states and couple with light polarized perpendicular to the stress axis (σ polarization). One point, however, is interesting to outline. In the first 2×2 matrix, the forbidden $|2,1^+\rangle$ state couples with the $|X\rangle$ dipole-allowed state only through the kinetic part of the Hamiltonian. Consequently, the corresponding eigenstate is dipole allowed only at very low stress and becomes forbidden when the applied stress separates the two states. As a consequence, only one single component appears to be dipole allowed for π polarization at high stress. Conversely, the second 2×2 matrix clearly shows that the two basis states are both k and X coupled. As a result two components are dipole allowed in σ polarization.

The four eigenstates which couple with light are

$$E_{1,2}=\tfrac{1}{2}(E_l+E_h+\delta)+A\pm\tfrac{1}{2}P\ , \tag{8a}$$

$$E_{3,4}=\tfrac{1}{2}(E_l+E_h+\delta)+A\pm\tfrac{1}{2}Q\ . \tag{8b}$$

The corresponding eigenfunctions are

$$|1\rangle=\alpha_1|X\rangle+\beta_1|2,1^+\rangle\ , \tag{9a}$$

$$|2\rangle=\alpha_2|X\rangle+\beta_2|2,1^+\rangle\ , \tag{9b}$$

$$|3\rangle=\alpha_3|Y\rangle+\beta_3|2,1^-\rangle\ , \tag{9c}$$

$$|4\rangle=\alpha_4|Y\rangle+\beta_4|2,1^-\rangle\ , \tag{9d}$$

where

$$\alpha_1^2=\tfrac{1}{2}\{1+[-(2\epsilon+\delta)-(E_l-E_h)/2]/P\}\ , \tag{10a}$$

$$\alpha_3^2=\tfrac{1}{2}\{1+[+(\epsilon+\delta)-(E_l-E_h)/2]/Q\}\ , \tag{10b}$$

$$\beta_j^2=1-\alpha_j^2,\quad \alpha_{j+1}=-\beta_j,\quad \beta_{j+1}=\alpha_j\quad (j=1,3)\ , \tag{10c}$$

with

$$P=[4\epsilon^2-4\epsilon\delta+\delta^2+(E_l-E_h)^2+(2\epsilon-\delta)(E_l-E_h)]^{1/2}, \tag{11a}$$

$$Q=[4\epsilon^2+2\epsilon\delta+\delta^2+(E_l-E_h)^2+(2\epsilon-\delta)(E_l-E_h)]^{1/2}. \tag{11b}$$

For a given component the oscillator strength depends on the value of $B_j=4\pi\beta_0\alpha_j^2$ ($j=1$—4), where $4\pi\beta_0$ is the interband oscillator strength which is related to the longitudinal-transverse splitting at $k=0$.

Figures 3 and 4 give the exciton dispersion curves and the corresponding ratio of oscillator strengths at $X=0$ and 20 bars. The parameters used in the calculation correspond to the best fit obtained in Sec. IV. The photon dispersion curve is plotted as a vertical line in Fig. 3. Clearly, Fig. 4 shows that, for $X\neq 0$, $\alpha_2^2\simeq 1$ and $\alpha_1^2\simeq 0$, only the d-like component is dipole allowed in π polarization. Since we know the exciton dispersion curves, let us now concentrate on the exciton-polariton modes.

B. Polariton and reflectivity spectra

In the material, the exciton-photon interaction gives rise to new normal modes of the system, the so-called excitonic polaritons which result from the admixture of excitonlike and photonlike states. From the exciton dispersion curve and the corresponding oscillator strengths, we calculate the polariton dispersion curve by the usual technique:[15]

$$\epsilon=\epsilon_\infty+\sum_j \frac{4\pi B_j(k)\omega_j^2(k)}{\omega_j^2(k)-\omega^2-i\omega\Gamma_j} . \tag{12}$$

As shown by Eq. (9), there are two exciton dispersion branches made from the $|X\rangle$ dipole-allowed component, labeled $|1\rangle$ and $|2\rangle$, and two branches made from the $|Y\rangle$ state labeled $|3\rangle$ and $|4\rangle$. Of course, only $|1\rangle$ and $|2\rangle$ excitons couple with π-polarized photons, while $|3\rangle$ and $|4\rangle$ excitons couple with σ-polarized photons, so that

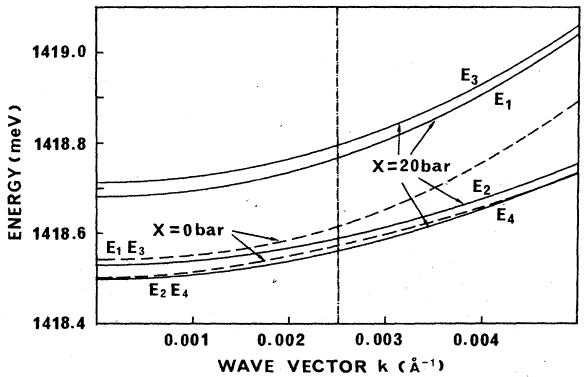

FIG. 3. Exciton dispersion curves at zero stress (dashed line) and under 20 bars [100] uniaxial stress (solid lines). The parameters used in the calculation are those giving the best fit in Sec. IV. Also shown is the photon dispersion curve (dashed-dotted line).

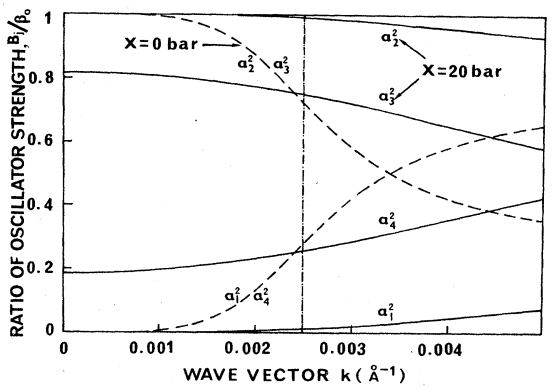

FIG. 4. k dependence of the relative oscillator strength at zero stress (dashed lines) and at $X=20$ bars (solid lines). Clearly, α_1^2 appears to be very small for the latter.

for each polarization, we deal with two exciton dispersion branches coupled with light. In this case Eq. (12) can be written as

$$\epsilon=\epsilon_\infty+\frac{4\pi\beta_0\alpha_j^2(k,X)\omega_j^2(k,X)}{\omega_j^2(k,X)-\omega^2-i\omega\Gamma_j}+\frac{4\pi\beta_0\alpha_{j+1}^2(k,X)\omega_{j+1}^2(k,X)}{\omega_{j+1}^2(k,X)-\omega^2-i\omega\Gamma_{j+1}} , \tag{13}$$

where $j=1$ and 3 for π and σ polarization, respectively. ϵ_∞ is the background dielectric constant, $\omega_j=E_j(k,X)/\hbar$ are the eigenvalues given by Eq. (8), Γ_j is a real positive damping constant, and α_j are given by Eq. (10); $4\pi\beta_0$ is the full oscillator strength. $\omega_j(k,X)$ and $\omega_{j+1}(k,X)$ in the numerator of each term will be approximated by ω_0 since the variation of these terms are small with respect to that of $\alpha_j(k,X)$.

The transverse solutions for $\epsilon(\omega,k,X)$ are determined by identification with the photon dispersion curve:

$$n^2=\epsilon=\frac{c^2k^2}{\omega^2} , \tag{14}$$

which, entered in Eq. (13), leads to the frequency—versus—wave-vector polariton dispersion relation. For a given ω this equation is cubic in k^2 and leads to three transverse solutions which can propagate into the material. They correspond to the three polariton dispersion branches and, of course, to the three different indices of refraction.

Now Eq. (14) gives k as a function of n and ω. Substituting in Eq. (13) we obtain an equation cubic in $n^2(\omega)$. By using E_i, E_{i+1}, α_i, and α_{j+1} given by Eqs. (8) and (10), a numerical calculation of this equation gives three solutions, $n_1(\omega,X)$, $n_2(\omega,X)$, and $n_3(\omega,X)$, corresponding to the three transverse modes already discussed.

Once we know the three indices of refraction, we can compute the theoretical reflection curve. However, there are two other problems, which need discussion: first, the additional boundary conditions (ABC's) and second, the surface effects.

Suppose that a plane monochromatic wave, with electric field E_I, is incident on the semiconductor surface

from vacuum, and let E_R be the electric field of the reflected wave and E_1, E_2, E_3 the electric field of the transmitted waves. The usual Maxwell boundary conditions[15] express the conservation of the tangential component of **E** and the normal component of **D**:

$$E_I+E_R=E_1+E_2+E_3 , \tag{15a}$$

$$E_I-E_R=n_1E_1+n_2E_2+n_3E_3 . \tag{15b}$$

In the classical case, with only one mode of propagation in the medium, E_R/E_I can be calculated from these conditions. However, we deal with three modes of propagation, and these conditions do not determine unambiguously the reflected and transmitted fields from the knowledge of the incident field. Additional boundary conditions are needed. Many workers discussed the ABC's under various physical considerations.[16] The different ABC's are referred to as ABC1, ABC2, and ABC3. The most commonly used, ABC1, are due to Pekar (Ref. 17) and require that the total exciton polarization should vanish at the boundary; ABC2 (Ref. 18) require that the normal component of the derivative of the polarization should vanish and ABC3 (Ref. 19) generalize ABC1 and ABC2. We used ABC1. Now each of the three modes which propagate in the medium contribute partially to the polarization. Returning to the dielectric constant, we can write each contribution as

$$\epsilon_l^j(\omega)=\frac{\alpha_0\omega_0^2\alpha_j^2(n_l)}{\omega_j^2(n_l)-\omega^2-i\Gamma_j\omega} , \tag{16}$$

where $j=1$–4 refers to resonance frequencies and $l=1,2,3$ refers to the mode of propagation. $\omega_j^2(n_l)$ and $\alpha_j^2(n_l)$ are determined by Eqs. (8) and (10), in which k is replaced by $\omega n_l/c$ per each mode of propagation. We obtain the resulting polarization of the medium,

$$P_j(\omega)=\sum_l \epsilon_l^j(\omega)E_j(\omega) . \tag{17}$$

Then, for the two exciton branches, ABC1 can be written as

$$\epsilon_1^jE_1+\epsilon_2^jE_2+\epsilon_3^jE_3=0 , \tag{18a}$$

$$\epsilon_1^{j+1}E_1+\epsilon_2^{j+1}E_2+\epsilon_3^{j+1}E_3=0 , \tag{18b}$$

where $j=1$ for π polarization and 3 for σ polarization.

In connection with the additional boundary conditions we must include the effects of a surface layer of the crystal where the exciton does not contribute to the dielectric function. This exciton-free layer is the so-called "dead layer." Again, the problem of the physical behavior of an exciton near the surface has been investigated by various authors.[15,20–27] For the origin of the dead layer Hopfield and Thomas[15] (HT) first proposed the presence of an image-force barrier that originates from the repulsive interaction of the exciton with its electrical image when the exciton approaches the surface. At the boundary the repulsive potential is infinite and, deeper into the crystal, one should have a gradual change in the exciton parameter (energy and damping parameters) toward the bulk conditions. Since this inhomogeneous region near the surface is difficult to deal with, HT replace it with an homogeneous dead layer. This model essentially corresponds to a rectangular exciton-free layer with an abrupt change of the damping parameter. This model was further refined by introducing for the exciton a depth-dependent damping[24] or eigenenergies,[25] or both.[26] However, a conclusive description of an exciton approaching the surface is still an open question, since, in addition to these intrinsic origins, there may be extrinsic ones due, for instance, to surface space charges.[27] In fact, all results obtained with the refined model given above clearly show that for large-sized Wannier excitons the homogeneous dead layer first proposed by HT applies to a very good approximation by taking a depth d of about twice the exciton Bohr radius $d\simeq 2a_0$. We used this approximation with ABC1 applied at the depth d from the surface. This correlates to a three-layer model with the vacuum characterized by the refractive index $n=1$, the dead layer characterized by $n_0=\sqrt{\epsilon_\infty}$, where ϵ_∞ is the background dielectric constant and, at the depth $d\simeq 2a_0$, the bulk characterized by the three indices of refraction n_1,n_2,n_3 already discussed (see Fig. 5).

The reflection coefficients at interfaces 1-2 (surface) and 2-3 are given, respectively, by

$$r_{12}=(1-\epsilon_\infty^{1/2})/(1+\epsilon_\infty^{1/2}) , \tag{19a}$$

$$r_{23}=(\epsilon_\infty^{1/2}-\epsilon^{1/2})/(\epsilon_\infty^{1/2}+\epsilon^{1/2}) . \tag{19b}$$

Taking account of the multiple reflections in the dead layer the resulting reflection coefficient is given by

$$r=\frac{r_{12}+r_{23}e^{2i\theta}}{1+r_{12}r_{23}e^{2i\theta}} , \tag{20}$$

with $\theta=2\pi d/\lambda_m$, where λ_m is the wavelength in the dead layer, $\lambda_m=\lambda/\epsilon_\infty^{1/2}$.

Now, in order to obtain the coefficient $r_{23}=E_R/E_I$, we apply Maxwell's boundary conditions and ABC1 at the interface 2-3. Let $\gamma_j=E_j/E_I$ ($j=1,2,3$) and Eqs. (15) and (18) be written as

$$\gamma_1+\gamma_2+\gamma_3-r_{23}=1 , \tag{21a}$$

$$n_1\gamma_1+n_2\gamma_2+n_3\gamma_3+n_0r_{23}=1 , \tag{21b}$$

$$\epsilon_1^j\gamma_1+\epsilon_2^j\gamma_2+\epsilon_3^j\gamma_3=0 , \tag{21c}$$

$$\epsilon_1^{j+1}\gamma_1+\epsilon_2^{j+1}\gamma_2+\epsilon_3^{j+1}\gamma_3=0 , \tag{21d}$$

where ϵ_l^j are given by Eq. (16), and $j=1$ for π polarization and 3 for σ polarization. Equations (21) give

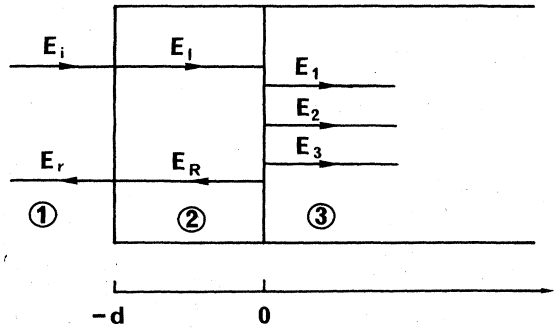

FIG. 5. Schematic picture of the three-layer model.

$$r_{23}=\frac{n_0-n_{\text{eff}}}{n_0+n_{\text{eff}}},$$

where n_{eff} is an effective index of refraction given by

$$n_{\text{eff}}=\frac{n_1\epsilon_{23}+n_2\epsilon_{31}+n_3\epsilon_{12}}{\epsilon_{12}+\epsilon_{23}+\epsilon_{31}},$$

with

$$\epsilon_{lk}=[\epsilon_k^j,\epsilon_l^{j+1}]=\epsilon_k^j\epsilon_l^{j+1}-\epsilon_l^j\epsilon_k^{j+1}.$$

III. EXPERIMENTAL TECHNIQUES

All experimental reflectivity spectra have been taken on very-high-purity [001] epitaxial layers of InP grown by vapor-phase epitaxy. We used a conventional PCl_3-In-InP process.[28] In this process the primary chemical reagents are hydrogen and phosphorous trichloride. The second reagent is indium metal. All reagents were used as obtained from the manufacturers and no further purification was attempted, except for hydrogen, which was purified by palladium diffusion units. The temperature achieved in the reaction tube was about 750 °C and that in the deposition zone was 650 °C. All substrates were single-crystal slices of InP mechanically polished in a 4% bromine-methanol solution. The typical layer thickness was about 10 μm.

We have investigated a series of ten different samples which all give similar results. From one sample to the other the main difference in optical spectra comes from the resolution of excitonic features associated with the $n=2$ excited state. This was better achieved with sample A (KV 296 in the nomenclature of Ref. 28), whose carrier concentration and electron mobility at liquid-nitrogen temperature were 8.6×10^{14} cm^{-3} and 70 000 cm^2/V s, respectively. Sample B (KV 322), for instance, whose mobility is higher and whose carrier concentration is lower (87 000 cm^2/V s and 2.8×10^{13} at 77 K, respectively) did not exhibit better-resolved features.

The uniaxial-stress experiments use a conventional stressing apparatus already described.[14] A lever arm lowers a stainless-steel rod which transmits the force to the sample chamber. The samples were obtained from the [001] epitaxial layer by cutting small rods along a [100] direction. After carefully polishing the narrow [100] pressure faces, this resulted in small parallelepipeds which were mounted between two optically flat pistons. A piezoelectric quartz transducer, positioned just below the sample, controlled the strength. Typical sample dimensions were $0.35\times1\times8$ mm^3, and the whole apparatus was designed to work in a pumped-liquid-helium bath.

The experimental configuration is given in Fig. 2. The photon wave vector **k** and the stress direction **X** were parallel to the [001] and [100] crystallographic axes, respectively. Both π and σ polarizations with respect to the stress direction were used. No important difference could be observed between spectra obtained on as-grown surfaces and after the sample had been chemically polished in a dilute solution of bromine in methanol.

IV. EXPERIMENTAL RESULTS

A typical reflectivity spectrum obtained at zero stress on our best sample is shown in Fig. 6. Clearly, we resolve

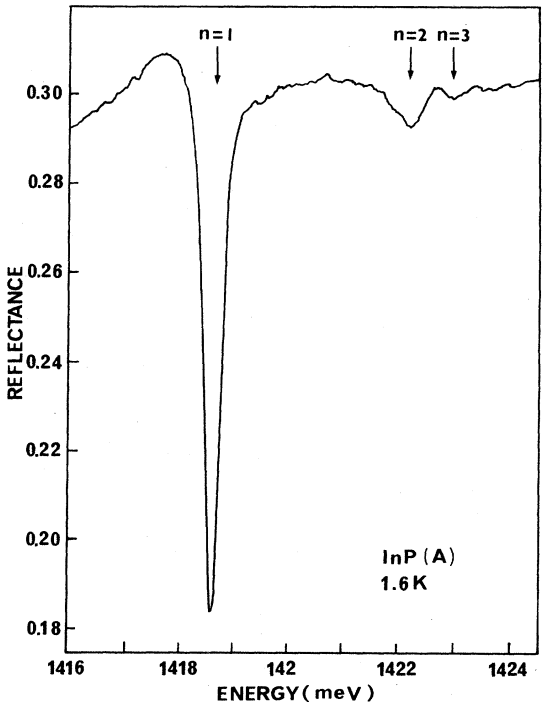

FIG. 6. Reflectivity spectrum obtained at pumped-liquid-helium temperature, without uniaxial stress (sample A).

three structures associated with the ground state and the two first excited excitonic states. From the difference between the energy minima we could deduce a crude estimate of the exciton binding energy. However, as discussed in Sec. II, the energy minima E_{mi} of the reflectance curve do not correspond exactly to the transverse-exciton energies E_{T1}, E_{T2}, and E_{T3}. Moreover, the energy difference E_{mi}-E_{Ti} depends on the oscillator strength, the damping parameter, and the dead-layer depth, all of which vary from the $n=1$ ground state to the $n=2$ or 3 excited states. Only a theoretical fit of the experimental spectra will permit one to obtain an accurate determination of the exciton binding energy.

This is done in Fig. 7, where we display for comparison the experimental and calculated reflectivity spectra in the vicinity of the $1s$ and $2s$ exciton resonances. Please note that a theoretical fit on the $3s$ excited stated is not significant. In this case, on account of the weakness of the oscillator strength, the structure is very small and the energies E_{m3}, E_{T3}, and E_{L3} are very close. Their determination does not need a fit: $E_{T3},=E_{L3}=E_{m3}$, within the experimental error. The calculated curve is obtained from the theory given in Sec. II. Among the different parameters used in the calculation, most were taken from experimental data and are listed in Table I. We have only adjusted the dead-layer thickness. For the $2s$ excited state the oscillator strength is the eighth of the ground state and we have used $\alpha_2=\alpha_0/8$.

The damping constant and the dead-layer depth have been taken as $\Gamma_2=0.2$ meV and $d_2=360$ Å, respectively. For each state, the longitudinal exciton energy E_L is defined as the energy of the polariton at $\mathbf{k}=\mathbf{0}$, where the

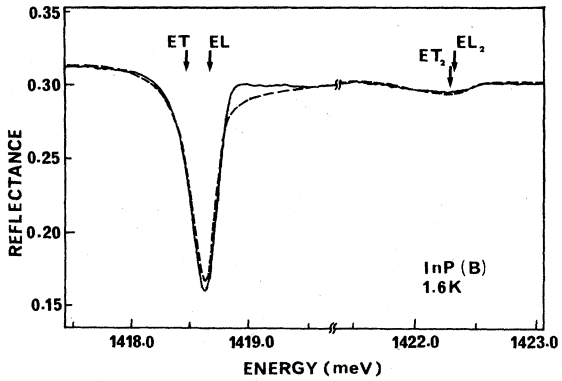

FIG. 7. Comparison of reflectivity spectrum (solid line) with a theoretical line-shape fit (dashed line) using the model given in Sec. II and the parameters given in Table I (sample B).

transverse upper polariton branch is degenerate with the longitudinal exciton. On the other hand, the transverse exciton energy E_T is defined as the energy of the $\mathbf{k}=\mathbf{0}$ exciton in the limit of zero exciton-photon interaction. These parameters are obtained by the usual relations $\epsilon^{-1}(\omega_T)=0$ and $\epsilon(\omega_L)=0$; the values calculated with the parameters given in Table I are $E_T=1418.50\pm0.05$ meV and $E_L=1418.67\pm0.07$ meV for the $1s$ ground state and $E_{T2}=1422.30+0.05$ meV and E_{L2} 1422.32 ± 0.07 meV for the $2s$ excited state. They are plotted in Fig. 7. We deduce the longitudinal-transverse splitting $E_{LT}=0.17\pm0.02$ meV and $E_{LT2}=0.02\pm0.02$ meV. Owing to the small oscillator strength of the $2s$ excited state, E_{LT2} is very small and the corresponding reflectance minimum is very close to the exciton-transverse energy. From the exciton-transverse energies we deduce an accurate value for the exciton binding energy, $E_{ex}=\frac{4}{3}(E_{T2}-E_T)$. We obtain

$$E_{ex}=5.1\pm0.1 \text{ meV} .$$

This value is to be compared with the results obtained by Bimberg *et al.*[29] from magnetoreflectance measurements (5.39 meV), by d'Andrea and Del Sole[30] from reflectance measurements (5.6 and 4.9 meV), and by Skolnick and Dean[31] from luminescence measurements (5 meV). Within experimental uncertainty, all values appear in satisfactory agreement. On the contrary, concerning the fine structure of excitons and because of the very small effects that one expects, only significant results can be obtained from a perturbative approach performed on very-high-quality crystals. This was the main goal of our work.

TABLE I. Best-fit parameters obtained for the $1s$ ground state and $2s$ excited state.

Parameter		$1s$	$2s$
Oscillator strength[a]	α_0	3×10^{-3}	$3/8\times10^{-3}$
Effective masses[b]	m_e	$0.08m_0$	
	γ_1	5.15	
	γ_2	0.94	
	γ_3	1.62	
Nondispersive dielectric constant[c]	ϵ_∞	12.36	
Damping parameter	Γ	0.06 meV	0.2 meV
Depth of the dead layer	d	180 Å	360 Å
Exchange energy	δ	0.04 meV	

[a]From experimental data of Ref. 35.
[b]From experimental data of Ref. 41.
[c]After Ref. 42.

Before discussing the parameters listed in Table I, let us present our results concerning the stress dependence of the reflectivity spectrum associated with the $1s$ ground state. Typical spectra obtained for [100] uniaxial compressions are shown in Fig. 8 for σ polarization. The solid lines correspond to experimental results and the dashed lines correspond to the calculated spectra. Figure 9 shows the stress dependence of the energy minimum of the structures where solid and open circles correspond to σ and π polarization, respectively. The solid lines correspond to the theoretical fit. Clearly, in the high-stress region we observe two structures in σ polarization and only one structure in π polarization. In π polarization (σ polarization) the structures are associated with the exciton branches $|1\rangle$ and $|2\rangle$ ($|3\rangle$ and $|4\rangle$) [Eqs. (9)], characterized by the resonance energies E_1 and E_2 (E_3 and E_4) [Eqs. (8)] and the oscillator strengths α_1^2 and α_2^2 (α_3^2 and α_4^2) [Eqs. 10)]. Owing to the fact that α_1 goes very rapidly to zero with increasing stress [see Eq. 10(a) and Fig. 4], the high-energy component in π polarization, $|1\rangle$, becomes dipole forbidden. In the low-stress region the situation is more complex because all the α_i ($i=1$–4) are not zero, but the splitting is very small and the structures are not clearly resolved. The calculated curves displayed in

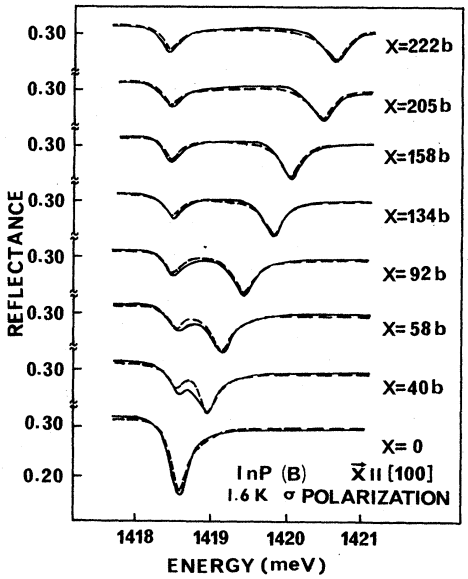

FIG. 8. Stress-induced behavior of the σ-polarization reflectivity spectrum. The stress is applied along the [100] crystallographic direction and the light is incident along the [100] axis. The solid lines correspond to experimental results. The dashed lines correspond to the theoretical fit obtained with the model given in Sec. II and the parameters given in Tables I and II.

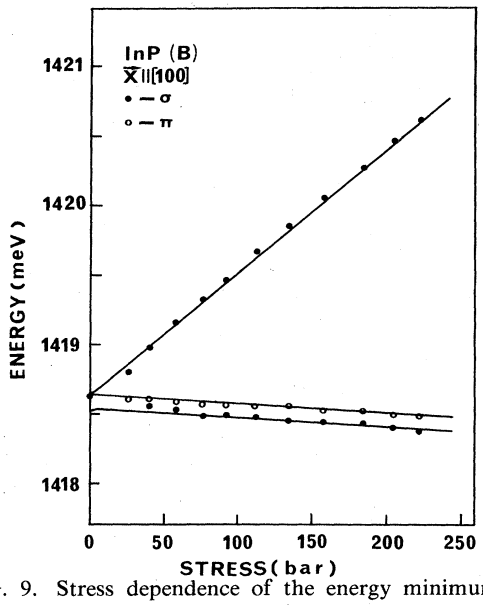

FIG. 9. Stress dependence of the energy minimum of the structures. Solid circles and open circles correspond to σ and π polarization, respectively. Solid lines correspond to theoretical fits.

Figs. 8 and 9 have been obtained with the parameters given in Table I and are discussed below. Only additional parameters characteristic of the stress-induced change in the band structure have been used. These new parameters are given in Table II. The hydrostatic and shear deformation potentials have been measured by different authors[32,33] and vary between 6 and 11 eV for a, and between -1.5 and -3 eV for b. The best fit in Fig. 9 has been obtained with the values quoted in Table II. In order to obtain the best fit in Fig. 8, it was necessary to account for the stress-induced broadening of the high-energy structure. Let us introduce a parameter which measures the strain inhomogeneity in the sample (μ); we find $\mu=3.0\times10^{-7}$ eV/bar, while the energy shift of the structure is 9.3×10^{-6} eV/bar. This corresponds to a stress inhomogeneity of about 3%, which is not very important.

V. DISCUSSION

Before discussing the values of the parameters used in the theoretical fit, let us note that these values permit fitting of the zero-stress reflectivity curve, the stress-induced shift of the reflectivity minima, and the line shape of the complete reflectivity spectra under various stress conditions. The damping parameter $\Gamma=0.06$ meV was obtained experimentally from the very-well-resolved luminescence spectra associated with the neutral-acceptor (A^0X) and neutral-donor (D^0X) —exciton complexes (see Fig. 4 of Ref. 5). These spectra and the corresponding value of Γ clearly show the good quality of the samples used.

TABLE II. Stress parameters.

Elastic compliance constant[a]	S_{11}	1.644×10^{-4} bar^{-1}
	S_{12}	-0.594×10^{-4} bar^{-1}
	S_{44}	2.174×10^{-4} bar^{-1}
Hydrostatic deformation	a	-9.3 eV
potential	a	-9.3 eV
Shear deformation potential	b	-2.1 eV
Broadening constant	μ	3×10^{-7} eV/bar

[a]After Ref. 32.

The polarizability parameter α_0 can be determined from the measured absorption coefficient at the band gap. For a nondegenerate hydrogenic exciton, the relation is[34]

$$4\pi\alpha_0=4\hbar c\epsilon_\infty^{1/2}R_0\alpha(E_g)/\pi E_g^2 ,$$

where R_0 is the exciton binding energy and $\alpha(E_g)$ is the absorption coefficient at the band-gap energy. Using our value for R_0 and, for $\alpha(E_g)$, the value measured on the curve given by Turner *et al.*,[35] $\alpha(E_g)\simeq1.1\times10^4$ cm^{-1}, we obtain $4\pi\alpha_0\simeq2.6\times10^{-3}$. The best fit has been obtained with $4\pi\alpha_0=3\ 10^{-3}$.

The effective masses of the light and heavy excitons have been calculated from Eqs. (66) and (67) of Ref. 11, as a function of the electron effective-mass and the Luttinger valence-band parameters. For the electron mass we have taken the value given by Chamberlain *et al.*,[36] $m_e=0.08m_0$. Concerning the Luttinger parameters, there exists in the literature a great deal of calculated[37–39] and experimental[40–43] values. Surprisingly, we find that the values proposed by Bimberg *et al.*[42] did not permit a good fit. The best fit was obtained using the values proposed by Rochon *et al.*:[41] $\gamma_1=5.15$, $\gamma_2=0.94$, and $\gamma_3=1.62$.

The dead layer has been chosen as an adjustable parameter, but its value is directly related to the Bohr radius of the exciton. The best fit has been obtained with $d=180$ Å; on the other hand, the calculated value of the exciton Bohr radius is of the order of 100 Å, and, consequently, the good fit is obtained with $d\simeq2a_0$. This result is in agreement with all the existing theories; moreover, it clearly shows the intrinsic nature of the exciton-free layer in our samples.

Lastly, concerning the exchange energy δ, we obtain $\delta=0.04\pm0.02$ meV. Now, from Eqs. (8), it is straightforward to show that, at high stress, the energy difference between E_4 and E_2 (the low-energy components allowed in σ and π polarization, respectively) tends to a constant value given by $4\delta/3$. This is not the energy difference measured on the reflectivity minima given in Fig. 9 (0.11 meV). Consequently, associating the reflectivity minima with E_4 and E_2, we would obtain $\delta=0.08$ meV. This value corresponds to the value, 0.07 meV, proposed by Weber *et al.*[33] from the energy shift of the minima of the reflection curve. This assignment is not exact because E_4 and E_2 correspond to transverse exciton energies and not to the minima of the reflection curve. Only a complete fit permits the deduction of δ from the stress dependence of the reflectivity curve. This results from the fact that the difference between the resonance energy and the reflectance minimum is not the same in σ and π polarization because the oscillator strengths are different. Now, as discussed in Sec. II, for Wannier excitons, δ corresponds almost exactly to the short-range contribution of the exchange energy Δ. Therefore, with a good approximation we can propose $\Delta=0.04\pm0.02$ meV. This value agrees with the one proposed by Ekart *et al.*[44] from polariton

spectra in an intermediate magnetic field. Concerning E_{LT}, only Ekart *et al.* have proposed an upper limit of about 0.1 meV. No other value is available for comparison.

VI. CONCLUSION

We have investigated the fine structure of the direct exciton in InP. At pumped-liquid-helium temperature, measuring the reflectivity spectrum at normal incidence, we have obtained three structures associated with the $1s$ ground state and $2s$ and $3s$ excited states of the exciton. From a careful analysis of the line shape, we deduce an accurate value of the exciton ionization energy, $E_{ex}=5.1\pm0.1$ meV. The structure associated with the $1s$ ground state is analyzed in terms of the three-branch polariton dispersion curve both at zero stress and under [100] uniaxial compression. We have used the model for the homogeneous dead layer and the additional boundary conditions proposed by Pekar (ABC1). We obtain a very good agreement between theory and experiment with a dead-layer depth of about twice the exciton Bohr radius. We deduce the exchange energy $\Delta=0.04\pm0.02$ meV and the longitudinal-transverse splitting $E_{LT}=0.17\pm0.02$ meV.

[1]For a recent review, see P. J. Dean and D. G. Herbert, in *Excitons,* edited by K. Cho (Springer, New York, 1979), p. 65.

[2]H. Mathieu, B. Archilla, P. Merle, and J. Camassel, Phys. Rev. B **20**, 4268 (1979).

[3]H. Mathieu, L. Bayo, J. Camassel, and P. Merle, Phys. Rev. B **22**, 4834 (1980).

[4]H. Mathieu, P. Merle, L. Bayo, and J. Camassel, Phys. Rev. B **22**, 4710 (1980).

[5]H. Mathieu, J. Camassel, and F. Benchekroun, Phys. Rev. B **29**, 3438 (1984).

[6]C. Weber and W. Ruhle, Phys. Status Solidi B **92** 425 (1979).

[7]J. Lagois, Phys. Rev. B **16**, 1699 (1977).

[8]T. Skettrup and I. Balslev, Phys. Status Solidi **40**, 93 (1970).

[9]R. S. Knox, *Theory of Excitons,* Suppl. 5 of *Solid State Physics,* edited by F. Seitz and D. Turnbull (Academic, New York, 1963).

[10]R. Bonneville and G. Fishman, Phys. Rev. B **22**, 2008 (1980).

[11]E. O. Kane, Phys. Rev. B **11**, 3850 (1975).

[12]M. Altarelli and N. O. Lipari, Phys. Rev. B **15**, 4898 (1977).

[13]B. Sermage and G. Fishman, Phys. Rev. B **23**, 5107 (1981).

[14]J. Altier, J. Camassel, and H. Mathieu, in *Proceedings of the International Conference on Measurement and Control: MECO, Zurich, 1977,* edited by M. H. Hanza (Acta, Zurich, 1977), p. 65.

[15]J. J. Hopfield and D. G. Thomas, Phys. Rev. **132**, 563 (1963).

[16]See, for instance, J. S. Nkoma, J. Phys. C **16**, 3713 (1983), and references therein.

[17]S. I. Pekar, Zh. Eksp. Teor. Fiz. **33**, 1022 (1958) [Sov. Phys.—JETP **6**, 785 (1958)].

[18]T. Skettrup, Phys. Status Solidi **60**, 695 (1973).

[19]J. Biellmann, M. Grossman, and S. Nikitine, in *Polaritons,* edited by E. Burstein and F. de Martini (Pergamon, Oxford, 1974), p. 183.

[20]G. S. Agarwal, D. N. Pattanayak, and E. Wolf, Phys. Rev. Lett. **27**, 1022 (1971).

[21]T. Skettrup and I. Balslev, Phys. Rev. B **3**, 1457 (1971).

[22]J. J. Sein, J. Opt. Soc. Am. **62**, 1037 (1972).

[23]F. Evangelisti, A. Frova, and F. Patella, Phys. Rev. B **10**, 4253 (1974).

[24]W. Ekart, K. Losch, and D. Bimberg, Phys. Rev. B **20**, 3303 (1979); J. Lagois, E. Wagner, W. Bendan, and K. Losch, Phys. Rev. B **18**, 4325 (1978).

[25]S. Satpathy, Phys. Rev. B **28**, (1983).

[26]J. Lagois, Phys. Rev. B **23**, 5511 (1981).

[27]L. Schulteis and I. Balslev, Phys. Rev. B **28**, 2292 (1983).

[28]K. Fairhurst, D. Lee, D. S. Robertson, H. T. Parfitt, and W. H. E. Wilgoss, J. Mater. Sci. **16**, 1013 (1981).

[29]D. Bimberg, K. Hess, N. O. Lipari, J. U. Fischback, and M. Altarelli, Physica **89B**, 139 (1977).

[30]A. d'Andrea and R. Del Sole, Phys. Rev. B **25**, 3714 (1982).

[31]M. S. Skolnick and P. J. Dean, J. Phys. C **15**, 5863 (1982).

[32]J. Camassel, P. Merle, L. Bayo, and H. Mathieu, Phys. Rev. B **22**, 2020 (1980).

[33]G. Weber and W. Ruhle, Phys. Status Solidi B **92**, 425 (1979).

[34]D. D. Sell, S. E. Skakouski, R. Dingle, and J. V. Dilorenzo, Phys. Rev. B **7**, 4568 (1973).

[35]W. J. Turner, W. E. Reese, and G. D. Petit, Phys. Rev. **136**, A1467 (1964).

[36]J. M. Chamberlain, P. E. Simmonds, R. A. Stradling, and G. L. Bradley, in Proceedings of the 11th International Conference on the Physics of Semiconductors, Warsaw, 1972 (unpublished), p. 1016.

[37]M. Cardona, J. Phys. Chem. Solids **24**, 1543 (1963).

[38]R. L. Bowers, and G. D. Mahan, Phys. Rev. **185**, 1073 (1969).

[39]P. Lawaetz, Phys. Rev. B **4**, 3460 (1971).

[40]J. Leotin, R. Barbaste, S. Askenazy, M. S. Skolnick, R. A. Stradling, and J. Tuchendler, Solid State Commun. **15**, 693 (1974).

[41]R. Rochon and E. Fortin, Phys. Rev. B **12**, 5803 (1975).

[42]D. Bimberg, K. Hess, N. O. Lipari, J. U. Fischback, and M. Altarelli, Physica **81B**, 139 (1977).

[43]W. Ekart, K. Losch, and D. Bimberg, Verh. Dtsh. Phys. Ges. **12**, 46 (1977).

[44]W. Ekart, K. Losch, and D. Bimberg, Phys. Rev. B **20**, 3303 (1979).